Atmos. Meas. Tech. Discuss., 2, 689–723, 2009
www.atmos-meas-tech-discuss.net/2/689/2009/

Atmospheric
Measurement
Techniques
Discussions

An experimental technique for the direct measurement of N_2O_5 reactivity on ambient particles

T. H. Bertram[1], **J. A. Thornton**[1], **and T. P. Riedel**[1,2]

[1]Department of Atmospheric Sciences, University of Washington, Seattle, WA, USA
[2]Department of Chemistry, University of Washington, Seattle, WA, USA

Received: 6 February 2009 – Accepted: 15 February 2009 – Published: 4 March 2009

Correspondence to: J. A. Thornton (thornton@atmos.washington.edu)

Published by Copernicus Publications on behalf of the European Geosciences Union.

Abstract

An experimental approach for the direct measurement of trace gas reactivity on ambient aerosol particles has been developed. The method utilizes a newly designed entrained aerosol flow reactor coupled to a custom-built chemical ionization mass spectrometer. The experimental method is described via application to the measurement of the N_2O_5 reaction probability, $\gamma(N_2O_5)$. Laboratory investigations on well characterized aerosol particles show that measurements of $\gamma(N_2O_5)$ observed with this technique are in agreement with previous observations, using conventional flow tube methods, to within ±20% at atmospherically relevant particle surface area concentrations (0–1000 $\mu m^2\,cm^{-3}$). Uncertainty in the measured $\gamma(N_2O_5)$ is discussed in the context of fluctuations in potential ambient biases (e.g., temperature, relative humidity and trace gas loadings). Under ambient operating conditions we estimate a single-point uncertainty in $\gamma(N_2O_5)$ that ranges between $\pm(1.3\times10^{-2}+0.2\times\gamma(N_2O_5))$, and $\pm(1.3\times10^{-3}+0.2\times\gamma(N_2O_5))$ for particle surface area concentrations of 100 to 1000 $\mu m^2\,cm^{-3}$, respectively. Examples from both laboratory investigations and field observations are included alongside discussion of future applications for the reactivity measurement and optimal deployment locations and conditions.

1 Introduction

Heterogeneous and multiphase reactions impact the magnitude and spatio-temporal distribution of trace gases and aerosol particles throughout Earth's atmosphere (Ravishankara, 1997). In the stratosphere, gas-surface reactions have received considerable attention due to their pivotal role in the catalytic destruction of ozone (O_3) (WMO, 1994). In contrast, the role of tropospheric heterogeneous and multiphase reactions continues to be assessed, building on recent advances in the measurement (Martin et al., 2008; Jayne et al., 2000; Murphy and Thomson, 1995) and model representation (Wang et al., 2008; Evans and Jacob, 2005) of the complex chemical composition, mixing state and phase of tropospheric particles.

The atmospheric lifetime of particles is directly impacted by heterogeneous reactions. Laboratory experiments have shown that heterogeneous oxidation of particulate organic matter (POM) has the potential to increase the hygroscopicity of the condensed phase (e.g., Broekhuizen et al., 2004), increasing particle loss via wet-deposition. In addition, evaporative loss of highly volatile products of POM oxidation leads to a decrease in atmospheric particulate loadings (Vlasenko et al., 2008; McNeill et al., 2008; Molina et al., 2004). Both of these processes decrease the atmospheric lifetime of particles and diminish their impact on the radiation budget and air quality. Heterogeneous processes can also play an important role in the gas-particle partitioning of volatile organic compounds, leading to the growth of secondary organic aerosol (Kroll and Seinfeld, 2005; Jang et al., 2002). In parallel, reactions occurring on particles can have a substantial impact on reactive trace gas budgets. For example, reactions of N_2O_5 occurring on or within aerosol particles have been estimated to account for 50% of tropospheric NO_x ($NO_x \equiv NO+NO_2$) removal (Dentener and Crutzen, 1993), while multiphase oxidation reactions of sulfur dioxide (SO_2) in cloud droplets has been proposed to account for a significant fraction of the total SO_2 loss (Calvert et al., 1985). As in the stratosphere, the products of tropospheric heterogeneous and multiphase reactions can play a critical role in tropospheric chemistry. For example, particulate chloride can be activated to the gas-phase as a labile Cl atom source following the uptake of N_2O_5 on chloride-containing particles (Osthoff et al., 2008; Thornton and Abbatt, 2005b; Behnke and Zetzsch, 1989; Finlayson-Pitts et al., 1989).

Laboratory investigations designed to determine the heterogeneous removal rate of trace gases have shown that reactive uptake on particles can be both rapid and highly variable, depending on particle chemical composition, phase, acidity and presence of surfactant coatings (George et al., 2007; McNeill et al., 2006; Laskin et al., 2006; Folkers et al., 2003; Thornton et al., 2003; Mentel et al., 1999; Abbatt and Waschewsky, 1998; Hu and Abbatt, 1997; Fried et al., 1994; Vogt and Finlayson-Pitts, 1994). However, several issues plague the quantitative extension of laboratory results to ambient conditions. For example, model laboratory systems may not accurately represent real ambient particles, due to the known complexity in tropospheric particle chemical composition, phase and mixing state. In addition, high gas and particle concentrations often used in laboratory experiments may require non-linear extrapolations to ambient conditions, due to processes such as surface saturation or amplification of second-order phenomena.

In the following manuscript we describe a new entrained aerosol flow reactor coupled to a custom-built chemical ionization mass spectrometer (CIMS) designed to directly measure the reaction probability of trace gases on ambient aerosol particles. We first discuss the technique in general terms applicable to a suite of gas-particle systems and then describe in detail the uncertainty, laboratory calibration and field deployment of the method in the context of N_2O_5 reactivity. Scientific results from the first in situ observations of N_2O_5 reactivity using this technique can be found in Bertram et al. (2009).

2 Gas-particle kinetics

2.1 Determination of k_{het} and γ by existing laboratory techniques

Laboratory investigations employing a continuous-flow reactor (tube) to study gas-particle reactions date to at least the work of Mozurkewich, et al. (1988). In this apparatus, the reactant gas is introduced into a particle-laden flow stream at various points along the length of the flow tube using a moveable injector thereby varying the gas-particle interaction time (Δt). The pseudo-first-order rate coefficient for reactant gas loss to particles (k_{het}) is then retrieved from fitting the measured decay in the gas concentration as a function of Δt. The quality of the derived k_{het} is largely determined by the magnitude of the particle-induced decay relative to non-particle induced losses (i.e. competing gas-phase reactions or wall interactions) and the stability of the reactant gas source.

To first-order, the magnitude of k_{het} (s^{-1}) can be related to the reaction probability (γ), for small particles (<200 nm) and low reaction probabilities (<0.1), via Eq. (1):

$$k_{\mathrm{het}} = \frac{\gamma \varpi S_a}{4} \tag{1}$$

where ϖ is the mean molecular speed ($\mathrm{m\,s^{-1}}$) of the reactant gas molecule and S_a ($\mathrm{m^2\,m^{-3}}$) is the particle surface area concentration. In laboratory studies, k_{het} can be driven to large values relative to other sinks by using S_a two to three orders of magnitude higher than typically observed in the atmosphere (S_a(ambient) $<1000\,\mu\mathrm{m}^2\,\mathrm{cm}^{-3}$). In this way, interaction times of minutes or less produce decays substantially greater than one e-fold even for $\gamma<0.01$. In addition, particle composition and loadings can be actively controlled often on time scales approaching hours. Consequently, in laboratory-based flow reactors, reactant decay can be mapped across several minutes with good precision. In contrast, to produce a one e-fold decay in the same manner using ambient S_a requires extended interaction times of several minutes at least. As a result, measurement of a full decay in a necessarily slow-flow reactor would take far longer than the typical time scales of atmospheric variability in the particle concentration and chemical composition. In theory, the problem of low ambient S_a could be addressed via particle pre-concentration, a technique commonly used to enhance particle mass loadings (Sioutas et al., 1995). However, the ambient S_a weighted mean particle diameter rarely exceeds 200 nm, making efficient concentration difficult without inducing a large pressure drop that has the potential to significantly alter particle chemical composition and/or phase (Boulter et al., 2006), and thus significantly affect the inferred γ.

To meet these challenges, we describe a novel application of reactant (particle) modulation in an extended interaction time flow reactor, making possible direct measurements of gas-aerosol interactions at ambient S_a concentrations. Our sampling routine to determine k_{het} relies solely on observations of the trace gas concentration (X) made at the base of the flow reactor in the presence and absence of aerosol particles.

2.2 Determination of k_{het} and γ by particle modulation

The integrated continuity equation for the pseudo-first-order loss of X in the presence and absence of particles, can be represented by Eqs. (2) and (3), respectively:

$$\ln\left([X]_{\Delta t}^{\mathrm{wo/particles}}\right) = \ln\left([X]_{t=0}\right) - \left(k_{\mathrm{wall}} + k_{\mathrm{hom}}\right)\Delta t \qquad (2)$$

$$\ln\left([X]_{\Delta t}^{\mathrm{w/particles}}\right) = \ln\left([X]_{t=0}\right) - \left(k_{\mathrm{wall}} + k_{\mathrm{hom}} + k_{\mathrm{het}}\right)\Delta t \qquad (3)$$

where $[X]_{t=0}$ and $[X]_{\Delta t}$ are the concentrations of X measured at the top and bottom of the flow reactor and k_{wall} and k_{hom} are the pseudo-first-order rate coefficients for reactions of X with the reactor walls and gas-phase species, respectively. Assuming that k_{wall} and k_{het} are constant between successive observations with and without particles and all losses of X are first-order in X, Eq. (2) can be substituted into Eq. (3) to formulate an equation for k_{het} that is dependent only on Δt and $[X]$ in the presence ($[X]_{\mathrm{w/aerosol}}$) and absence of particles ($[X]_{\mathrm{wo/aerosol}}$).

$$k_{\mathrm{het}} = -\left(\frac{1}{\Delta t}\right)\ln\left(\frac{[X]_{\Delta t}^{\mathrm{w/particles}}}{[X]_{\Delta t}^{\mathrm{wo/particles}}}\right) \qquad (4)$$

We use a time-dependent box model to determine the time scales and S_a required to measure k_{het} on ambient particles. Results from the box model simulations are shown in Fig. 1 for three representative reaction probabilities (γ=0.001, 0.01, and 0.1) as a function of S_a, where we assume $k_{\mathrm{wall}}=2.5\times10^{-3}\,\mathrm{s}^{-1}$. This k_{wall} is close to the inverse time scale for diffusion of gas molecules from the center to the walls of a 15 cm ID tube. The concentration at the base of the reactor ($[X]_{t=8\,\mathrm{min}}$) is shown in Fig. 1a relative to the initial concentration at the top of the flow reactor ($[X]_{t=0\,\mathrm{min}}$). The ratio of $[X]$ measured in the presence to that in the absence of particles, as a function of γ, is shown in Fig. 1b. The simulations highlight the fact that uncertainty in the derived k_{het} will be a function of the variability in k_{wall}, k_{hom}, S_a, and the output of the X source.

The results suggest that at particle exposure times ($S_a \times \Delta t$) of 8000 μm^2 cm^{-3} min, statistically significant measurement of γ to better than 0.001 requires certainty in k_{wall}, k_{hom} and stability in the X source to better than ±2%. At the limit of high reaction probability (γ>0.1), the experiment necessitates significantly shorter particle exposure times, to ensure that the decay in X remains first-order and the assumptions used in deriving Eq. (3) are not violated. To balance these requirements, we designed our reactor to have a Δt=8 min, thus targeting the detection of γ from 0.001 to 0.1 over the range of ambient S_a (0–1000 μm^2 cm^{-3}). A more rigorous, species specific treatment of uncertainty is discussed in Sect. 4.

The reaction probability is then calculated directly from the measured k_{het}, following correction for non-plug flow conditions (Brown, 1978), and co-located observations of S_a via Eq. (4):

$$\frac{1}{\gamma} = \frac{\varpi S_a}{4k_{\mathrm{het}}} - \frac{0.75 + 0.283\overline{K_n}}{\overline{K_n}(1 + \overline{K_n})}, \tag{5}$$

where

$$K_n = \frac{3\,D_g}{\varpi \overline{r_s}}, \quad \overline{r_s} = r_p \exp\left(2.5\,(\ln\sigma)^2\right)$$

where D_g is the gas-phase diffusion coefficient (m^2 s^{-1}) for species X and r_p and $\ln\sigma$ describe the radius and width of the log-normal particle size distribution, respectively (Hanson and Kosciuch, 2003; Fuchs and Sutugin, 1970).

3 Application to direct measurements of γ(N_2O_5)

The preceding discussion is generally applicable to any gas-particle reactive system. To illustrate the viability of the concept we describe its application to the first direct in situ measurements of N_2O_5 reactivity, and thus determinations of γ(N_2O_5), on ambient

Title Page
Abstract Introduction
Conclusions References
Tables Figures
◀◀ ▶▶
◀ ▶
Back Close
Full Screen / Esc
Printer-friendly Version
Interactive Discussion

aerosol particles. Laboratory studies have shown that the reactive uptake of N_2O_5 is both first-order in N_2O_5 and is highly variable ($5\times10^{-4}<\gamma N_2O_5<0.03$), stemming from a strong dependence on: i) particle liquid water content (Thornton et al., 2003), ii) particle nitrate mole fraction, which inhibits N_2O_5 hydrolysis (Mentel et al., 1999; Wahner et al., 1998), iii) organic coatings that have been theorized to either suppress N_2O_5 accommodation or decrease water availability at the surface (Cosman and Bertram, 2008; Cosman et al., 2008; Park et al., 2007; McNeill et al., 2006; Badger et al., 2006; Thornton and Abbatt, 2005b; Folkers et al., 2003), and iv) particle acidity (Hu and Abbatt, 1997; Robinson et al., 1997; Fried et al., 1994; Mozurkewich and Calvert, 1988). The complex dependence of $\gamma(N_2O_5)$ on particle chemical composition and phase presents both a test and a clean case of need for the direct measurement of $\gamma(N_2O_5)$ on ambient particles.

3.1 Entrained aerosol flow reactor

3.1.1 Filter manifold

A schematic of the entrained aerosol flow reactor and particle filter manifold, designed to meet the aforementioned requirements, is shown in Fig. 2. Ambient air is sampled through a 30 cm long, 0.95 cm inside diameter (ID) aluminum inlet, where the inlet tip is curved (5 cm radius of curvature) at 180° relative to vertical, to reject large droplets. Ambient air is then either introduced directly into the flow reactor or first diverted through a PTFE membrane (Pall Life Sciences) to remove particles. The filter medium was chosen as a balance between minimizing both the pressure drop and relative humidity (RH) difference between filter inline and filter bypassed states, while maintaining high particle collection efficiency. A double-acting pneumatic actuator, coupled to two parallel 0.95 cm ID stainless-steel ball valves, was used to modulate the flow direction between the filter inline and bypassed states.

3.1.2 Flow reactor

The primary section of the flow reactor is comprised of a 15 cm ID stainless-steel tube, 90 cm in length. Flow enters and exits the tube via 5 cm deep 60° tapered aluminum end caps. The reactor interior walls and end caps are coated with halocarbon wax (Series 1500 Inert Wax, Halocarbon Products Corp.) to minimize wall reactions, while maintaining high particle passing efficiencies. The exterior of the flow reactor is insulated with aluminum coated 1″ polyethylene foam to minimize thermal eddies resulting from differential heating of the exterior of the tube. The reactant gas is added to the ambient sample stream prior to injection into the flow reactor. The reaction mixture is then introduced perpendicular to the flow direction of the reaction chamber via a side port on the aluminum entrance cap. The orthogonal entry is designed to facilitate turbulent mixing and to minimize the entrance length of the injected flow. Introduction of the flow tangentially to the conical entrance cap will likely improve mixing and laminar flow development.

The reaction temperature, pressure and RH are determined by the ambient conditions and monitored at the base of the reactor. The volumetric flow rate of the reactor is set by the sampling rates of the gas and particle measurements made at the base of the flow reactor. For example, a flow rate of 2000 sccm results in a linear flow velocity of 0.19 cm s^{-1} and an average residence time of 480 s. We use the responses of the S_a and reactant gas concentration (here N_2O_5) measured at the base of the flow reactor to determine the time required to reach a new steady-state following a change in the filter state at the top of the flow reactor (Fig. 3). These measurements confirm an average reaction time of 8 min. The absence of a clear step function in the response is indicative of non-plug flow conditions and suggests that the interaction time used in this analysis represents an average residence time rather than a finite interaction time. As a result, the described technique is better characterized as a hybrid of a static reaction chamber and a fully developed, well characterized laminar flow tube. Uncertainty introduced by the effects of non-plug flow, diffusion limitations and secondary chemistry are assessed in Sect. 4.

3.1.3 Particle transmission

The passing efficiency of aerosol particles through the flow reactor was evaluated in detail using laboratory-generated particles and assessed routinely on ambient particles during field deployment. In the laboratory, malonic acid (MA) particles were generated by homogeneous nucleation. The resulting particle size distributions, as measured at the top (black) and bottom (dark gray) of the flow reactor are shown in Fig. 4a. The total particle number concentration in this example was conserved to within 95%, while the total S_a concentration measured at the base of the flow reactor was approximately 75% of that measured at the top of the flow reactor. This is most likely due to evaporation of either water or MA from the particle after injection into the flow reactor. Observations of the passing efficiency of ambient particles routinely displayed less than 10% loss in total S_a. Particle filter break-through was also measured routinely during field deployment. The size distribution, as measured at the base of the flow reactor when sampling through the filter is also shown Fig. 4a (light gray). As shown by the size distribution, the PTFE filter membranes operated at 2 slpm are not absolute filters, but they are more than sufficient for this application, removing >99% of the available S_a.

3.2 N_2O_5 generation

N_2O_5 was generated in situ in a secondary flow tube via the reaction of ozone (O_3) with excess nitrogen dioxide (NO_2) and subsequent reaction of the resultant nitrate radical (NO_3) with NO_2 via Reactions (R1)–(R2).

$$O_3 + NO_2 \rightarrow NO_3 + O_2 \qquad (R1)$$

$$NO_3 + NO_2 + M \leftrightarrow N_2O_5 + M \qquad (R2)$$

O_3 was generated from the photolysis of molecular oxygen (O_2) in compressed ultrapure zero air. In this application, a low-pressure mercury lamp (Jelight Company, Inc.)

was shielded from the N_2/O_2 flow stream by a custom-built variable aperture aluminum sheath, permitting fine adjustment of the O_3 mixing ratio (200–2000 ppbv). The O_3-laden flow (90 sccm) was then combined with 10 sccm of trace NO_2 in N_2 delivered from a NIST traceable compressed gas standard (10 ppmv, Scott-Marrin specialty gases). The reactants were mixed in a 1″ ID PFA-Teflon tube for 2 min prior to export to the entrained aerosol flow reactor. Following 20:1 dilution into the flow reactor, typical initial concentrations at the top of the flow reactor were: $[NO_2]_{t=0}$=50 ppbv, $[O_3]_{t=0}$=10 ppbv, $[N_2O_5]_{t=0}$=1 ppbv, and N_2O_5/NO_3 was greater than 50 at room temperature due to excess NO_2. The N_2O_5 generation system was purged with dry air for 24 h prior to injection of NO_2 to remove H_2O from the reactor surfaces and minimize nitric acid (HNO_3) production. HNO_3 from the generation source was monitored via CIMS and on average was less than 10% of N_2O_5, assuming similar iodine cluster ion formation rates for N_2O_5 and HNO_3 (Kercher et al., 2009). The resulting generation system, post dilution, is capable of producing N_2O_5 at atmospherically relevant mixing ratios (0–5 ppbv). Measurement of the change in O_3 following NO_2 addition provides a quantitative constraint on the magnitude of N_2O_5 produced. For the undiluted source, the observed change in O_3 agrees with that predicted by a time-dependent chemical box model to within ±20% (Fig. 5). The amount of N_2O_5 delivered ultimately depends on wall losses and temperature during transit. These factors can be assessed and monitored routinely, and thus this N_2O_5 source is expected to become a routine calibration method for future deployments of the N_2O_5 CIMS.

3.3 N_2O_5 detection

As described in detail in Kercher et al. (2009), N_2O_5 was detected as $I(N_2O_5)^-$ by CIMS using iodide (I^-) as the reagent ion. Briefly, reagent ions were generated by flowing trace methyl iodide (CH_3I) in N_2 over a radioactive ^{210}Po source. The reagent gas flow (2500 sccm) was combined with the sample flow (2000 sccm) and permitted to react for ~70 ms at 60 torr, prior to being guided through a series of ion lenses and focused into a quadrapole for mass selection and subsequent detection with an off-axis electron multiplier detector (Extrel Inc.). The resulting instrument achieves a detection threshold of 1 pptv min^{-1}, with a zero uncertainty of 5 pptv. The absolute accuracy of the instrument is set by the calibration method and is estimated to be ±20% for the N_2O_5 source described above. The low detection threshold and chemical specificity of the I^- CIMS enables us to conduct the experiment at atmospherically relevant mixing ratios ($[N_2O_5]<5$ ppbv), minimizing potential artifacts associated with working at high concentrations (e.g., Thornton et al., 2003).

3.4 N_2O_5 wall loss

Minimizing the magnitude and the variability in $k_{\mathrm{wall}}(N_2O_5)$ is critical for the accurate retrieval of k_{het}. Due to low ambient S_a and long Δt, the surface area of the flow reactor is often more than three orders of magnitude larger than the ambient S_a. As described in detail in the next section, minimizing short-term variability in k_{wall} is more important than the absolute magnitude of k_{wall}. The choice of wall coating is a compromise between particle and gas-phase passing efficiency. The ideal choice for minimizing k_{wall} would likely be extruded PFA-Teflon, however its non-conductive nature permits the build up of static charge that greatly increases particle loss rates. Halocarbon wax exhibited the best combination of high particle transmission and low N_2O_5 loss. In addition, the reactor walls were rinsed with distilled water every few days to remove deposited soluble material, which may act to increase the hygroscopicity of the walls. The magnitude of $k_{\mathrm{wall}}(N_2O_5)$ was determined daily in the field, by measuring the loss of N_2O_5 in the absence of particles. As expected, $k_{\mathrm{wall}}(N_2O_5)$ is a strong function of RH. The RH dependence of $k_{\mathrm{wall}}(N_2O_5)$, where the absolute magnitude varies between $0.5–3\times10^{-3}\,\mathrm{s}^{-1}$ for RH of 0 to 50%, is shown in Fig. 4b. We discuss the impacts of the $k_{\mathrm{wall}}(N_2O_5)$ RH dependence on the retrieval of $\gamma(N_2O_5)$ below.

4 Sources of uncertainty in k_{het}(N_2O_5) and γ(N_2O_5)

Ideally, the uncertainty in k_{het} is determined by the short-term variability in the N_2O_5 generation source. The minimum statistically significant difference between $[N_2O_5]_{w/aerosol}$ and $[N_2O_5]_{wo/aerosol}$ is set by the variance in the N_2O_5 source on the time scale of the sampling sequence (50 min). Laboratory measurements of the N_2O_5 source, made over a 12 h sampling window, reveal that sequential 10 min averages in the N_2O_5 signal are precise to within ±1%. Taking ±2% as the minimum statistically significant difference between N_2O_5 detected with and without particles, we calculate an uncertainty in k_{het} of $\pm 4\times10^{-5}\,s^{-1}$. This translates into a single-point uncertainty in $\gamma(N_2O_5)$ of $\pm 6.8\times10^{-3}$ for S_a=100 $\mu m^2\,cm^{-3}$, decreasing to $\pm 6.8\times10^{-4}$ for S_a=1000 $\mu m^2\,cm^{-3}$. However, in field sampling, additional and potentially more significant sources of uncertainty exist: i) production of N_2O_5 in the flow reactor, ii) gas and particle reactivity of NO_3, iii) RH dependent variations in k_{wall}, and iv) non-plug flow conditions.

4.1 In situ N_2O_5 production

Following dilution into the flow reactor, the initial concentrations of NO_2, O_3 and N_2O_5 are typically on the order of 50, 10, and 1 ppbv, respectively. Post injection, N_2O_5 continues to be produced in the flow reactor via Reactions (R1)–(R2). Figure 6 depicts the time dependence in N_2O_5 within the flow reactor as a function of k_{wall} and k_{het} as predicted with a comprehensive box model of nocturnal nitrogen oxide chemistry, in which we arbitrarily choose a $\gamma(N_2O_5)$. As shown, minor net production of N_2O_5 is observed in the flow reactor when k_{wall} equals zero. To assess the effect of production on our retrieved $\gamma(N_2O_5)$, we derive $\gamma(N_2O_5)$ using model predicted $[N_2O_5]$ at Δt=8 min in the presence and absence of particles via Eq. (3) and compare it with the true value (γ_{true}) prescribed in the model. In the extreme case where $[NO_2]_{t=0}$=100 ppbv and $[O_3]_{t=0}$=50 ppbv, the ratio method (Eq. 3) underestimates $\gamma(N_2O_5)$ by at most 10%.

4.2 NO_3 reactivity

The flow reactor was operated at high NO_2 concentrations to chemically shift the N_2O_5-NO_3 equilibrium in favor of N_2O_5, in order to minimize the effect of NO_3 loss processes on the retrieved $\gamma(N_2O_5)$. Yet, both gas and condensed phase reactions involving NO_3 can affect the N_2O_5 reactivity measurement. Gas-phase reactions between NO_3 and nitric oxide (NO) or volatile organic compounds (VOC) are likely more rapid than heterogeneous reactions and pose a potentially large challenge even at the high N_2O_5/NO_3 used. However, similar to wall losses of either N_2O_5 or NO_3, the homogeneous reaction rate is expected to be largely independent of the filter state and is thus a separable term in our analysis (Eqs 2–4). Therefore, only strong atmospheric variations in NO or VOC on the time scale of the sampling sequence will affect the N_2O_5 reactivity measurement. Using a time-dependent box model for the intial conditions used in the previous section, we estimate that our system is buffered against changes in VOC and NO up to 1 ppbv, where we assume an NO_3 reaction rate with VOC equal to that of isoprene. Despite the fact that $k_{\mathrm{NO+NO_3}}$ is much faster than $k_{\mathrm{Isoprene+NO_3}}$ (2.6×10^{-11} as compared with 7×10^{-13} cm^3 molecules^{-1} s^{-1} at 298 K (Atkinson and Arey, 2003)), we are approximately equally sensitive to both VOC and NO, because NO is partially removed from the flow reactor via O_3 titration. Thus, the extent to which we are sensitive to NO is also a function of the available O_3.

In contrast to gas-phase reactions of NO_3, reactive uptake of NO_3 to particles is inseparable to that from N_2O_5 and must be included in the error analysis. Again we use the time-dependent model to assess the impact of NO_3 uptake on the derived $\gamma(N_2O_5)$ for N_2O_5/NO_3=50, and a range of $\gamma(N_2O_5)$ and $\gamma(NO_3)$. In regions of high N_2O_5 reaction probability ($\gamma(N_2O_5)=0.05$, $S_a=200\,\mu m^2\,cm^{-3}$), our approach would overestimate $\gamma(N_2O_5)$ by at most 35% for the full range of possible $\gamma(NO_3)$. For example, model results indicate that for a true $\gamma(N_2O_5)$ of 0.05, the retrieved $\gamma(N_2O_5)$ would be 0.067, 0.051, and 0.05 for $\gamma(NO_3)$ of 1.0, 0.1 and 0.001, respectively. In contrast, regions of low N_2O_5 reactivity ($\gamma(N_2O_5)=1\times10^{-3}$, $S_a=200\,\mu m^2\,cm^{-3}$), our measurement is very sensitive to $\gamma(NO_3)$. Under these situations, model results show that the retrieved $\gamma(N_2O_5)$ would be increased from the true value of 0.001 to 0.019, 0.0032, and 0.001 for $\gamma(NO_3)$ of 1.0, 0.1 and 0.001, respectively.

In summary, our technique is buffered against minor changes in NO_3 gas-phase reactants and largely insensitive to $\gamma(NO_3)$ less than 0.1. However, for $\gamma(NO_3)>0.1$, our observations represent an upper limit for $\gamma(N_2O_5)$. While it is unlikely that $\gamma(NO_3)$ is uniformly greater than 0.1, recent laboratory measurements suggest that $\gamma(NO_3)$ could be large ($\gamma(NO_3)>0.1$) on fresh soot (Gross and Bertram, 2008; Mak et al., 2007). By routinely shifting the N_2O_5-NO_3 ratio to higher NO_3, via reducing NO_2 in the source, our approach can theoretically elucidate both N_2O_5 and NO_3 reactivity on particles.

4.3 RH dependent variability in k_{wall}

As shown in Sect. 2, our retrieval of k_{het} is independent of the magnitude of k_{wall}. However, variability in k_{wall} on the time scale of the sampling sequence can introduce additional uncertainty into the analysis. Successive determinations of k_{wall} are a measure of the temporal drifts in the wall loss rate due to changes in RH and aerosol accumulation on the walls, and provide an additional bound on the certainty of our retrieved k_{het}. As shown in Fig. 4b, changes in RH result in significant changes in k_{wall}, and stress the importance of maintaining constant RH at least between the filter inline and filter bypassed states. Measurements of RH performed at the base of the flow reactor provide direct insight on the variation in k_{wall} between filter states. These observations show that on average measurements of RH with the filter inline and bypassed agree to within ±2%, which is the stated measurement uncertainty in the RH probe. Figure 4b also highlights the decreasing sensitivity of k_{wall} to RH at high RH. As a result, at 10% RH, a ±1% change in RH would yield an uncertainty in k_{het} comparable to that of the N_2O_5 source ($5\times10^{-5}\,s^{-1}$), while at 50% RH a ±3% change would produce a similar uncertainty. The uncertainty in the derived k_{het} is thus primarily a function of the N_2O_5 source stability at high RH, but can become limited by RH fluctuations at low RH.

4.4 Non-plug flow conditions

As mentioned above, the physical dimensions and flow conditions of the reactor create non-ideal flow, leading to an average, rather than finite, reaction time (Fig. 3). Brown developed a routine to correct rate coefficients measured in tubular flow reactors for the effects of radial and axial diffusion under the assumption of fully developed laminar flow (Brown, 1978). It is unlikely that this method is applicable to our system. However, its application suggests, for our reactor and flow conditions, that the measured k_{het} would underestimate the true value by at most 25%. We expect our results depend only on the average reaction time, as measured by the time decay in N_2O_5 observed at the base of the reactor.

4.5 Estimated total uncertainty in $\gamma(N_2O_5)$

Incorporating all of these factors, we estimate an upper limit for the combined uncertainty in k_{het} of $\pm(8\times10^{-5}\,\mathrm{s}^{-1}+0.2\times k_{\mathrm{het}})$. This translates into a combined single-point uncertainty in $\gamma(N_2O_5)$, ranging between $\pm(1.3\times10^{-2}+0.2\times\gamma(N_2O_5))$ and $\pm(1.3\times10^{-3}+0.2\times\gamma(N_2O_5))$ for S_a concentrations of 100 to 1000 $\mu\mathrm{m}^2\,\mathrm{cm}^{-3}$, respectively. For a population of measurements, the random component of the uncertainty can be represented as the standard deviation of the mean of the observations, thus permitting analysis at lower S_a and $\gamma(N_2O_5)$ for a large collection of observations made on similar particle types. In air masses characterized by high NO or VOC variability, rapidly changing RH, or large $\gamma(NO_3)$ (>0.1), measurements of $\gamma(N_2O_5)$ will likely be unreliable. Co-located measurements of NO and RH provide the necessary tools to distinguish these events from statistically significant measurements. In light of these restrictions, ambient observations of $\gamma(N_2O_5)$ are likely most accurate in well-mixed air-masses characterized by low and slowly varying NO and VOC, and reasonably constant RH.

5 Laboratory demonstrations

Prior to field deployment, the N_2O_5 reactivity technique was investigated in the laboratory using particles for which $\gamma(N_2O_5)$ has been previously determined by traditional gas-particle kinetics techniques (Thornton et al., 2003; Folkers et al., 2003). In this experiment MA particles, generated via homogeneous nucleation, were diluted and conditioned to the desired S_a and RH prior to injection into the flow reactor. Particle S_a was varied between 0 and 1500 $\mu m^2\,cm^{-3}$ to reproduce atmospherically relevant S_a. The experiment was conducted at two different RH's to probe $\gamma(N_2O_5)$ on both aqueous (RH=50%) and crystalline (RH<5%) particles (Braban and Abbatt, 2004).

The particle modulation technique, described in Sect. 2, was employed in the same manner used for ambient observation. The sampling sequence is shown in detail in Fig. 7, where modulation in the S_a concentration is shown in the top panel and the resulting changes in N_2O_5 signal are shown in the bottom panel. The laboratory sampling sequence consists of: i) a 10 min averaging block with the filter inline (grey squares), ii) a 15 min equilibration time following the switch to unfiltered air, iii) a 10 min averaging block with the filter bypassed (black circles), and iv) a 15 min equilibration time following the switch to particle free air. Adjacent filter inline states are interpolated (dashed black line) to determine an appropriate $[N_2O_5]_{wo/aerosol}$ value for calculating k_{het}. The resulting sampling routine produces a unique measure of k_{het} every 50 min, while only requiring that particle loadings and chemical composition be constant for 10 min.

Results from the MA experiments are shown in Fig. 8a, where k_{het} is plotted against the measured S_a at the base of the flow reactor. As described by Eq. (4), the slope of the weighted linear least squares fit is a direct measure of $\gamma(N_2O_5)$. As shown in Fig. 8a, we calculate a $\gamma(N_2O_5)$ of 0.035 and 0.0012 for RH=50% and <5%, respectively. These values agree with those reported by Thornton et al. to within ±20% and demonstrate that the aforementioned experimental technique is capable of measuring $\gamma(N_2O_5)$ at atmospherically relevant S_a concentrations and N_2O_5 reaction probabilities characteristic of the troposphere (Brown et al., 2006).

6 Field performance

During the summer of 2008, the continuous flow reactor was deployed at two sampling locations; Boulder, CO and Seattle, WA. The scientific results of these studies are described in Bertram et al. (2009). Below, we describe the operation and performance of the N_2O_5 reactivity apparatus during the first field deployment to Boulder in July 2008. This deployment presented some unique challenges that illustrate the performance related issues described above.

For the Boulder experiments, the flow reactor was mounted to a 10 m tower adjacent to a temperature controlled sampling container that housed the CIMS instrument and co-located observations of particle chemical composition (Aerodyne compact time-of-flight aerosol mass spectrometer), particle size distributions (ultra-high sensitivity aerosol spectrometer), NO, O_3, and a series of standard meteorological parameters. The reactor was mounted to the tower to maintain ambient temperature and RH, while minimizing particle losses during inlet transmission. The reactant gas was generated, as described in Sect. 3.2, in the temperature controlled sampling container to minimize thermal fluctuations that may induce variability in the N_2O_5 output, before being delivered to the flow reactor via 15 m of 1/8″ Teflon tubing. The concentration of reactant gas at the base of the flow reactor was measured via a 15 m length of Teflon tubing (0.5 s transit time).

In Fig. 9 we show raw N_2O_5 signal during a typical sampling cycle under ambient conditions. Note that the reaction time in this example was extended slightly longer than the more typical 8 min by decreasing the CIMS sample flow rate. The sampling cycle, as operated in the field, consists of a seven-step sequence:

i) The sample flow was directed through the inlet filter and the reactant gas was measured and averaged for ten minutes to determine $[N_2O_5]_{wo/aerosol}$.

ii) Following filter removal at $t=10$ min, the observed N_2O_5 decays in accordance to the mixing time scales of the flow reactor. This data is not used in the determination of k_{het}, however the shape of the decay, as shown in dashed black lines, provides confidence that the observed difference is due to particle-associated changes rather than brief pulses of reactive trace gases.

iii) Following equilibration, a mass scan (30–250 amu) is performed in the presence of particles.

iv) N_2O_5 is measured and averaged for ten minutes in the presence of particles to determine $[N_2O_5]_{w/aerosol}$.

v) The sample flow stream is directed through the filter and the flow reactor is allowed to equilibrate to the new steady-state.

vi) A second mass scan is recorded in the absence of particles for comparison with the mass scan retrieved in step C. Using the scans obtained in steps C and F, a difference spectrum is created for analysis of species (detectable by I^- CIMS) that are lost (e.g., N_2O_5, HNO_3) or produced (e.g., $ClNO_2$, HONO) via particle reactions in the flow reactor.

vii) A second measure of $[N_2O_5]_{wo/aerosol}$ is performed to assess drift in k_{wall}. The two measurements of $[N_2O_5]_{wo/aerosol}$, obtained in steps A and G were then interpolated to determine the value of $[N_2O_5]_{wo/aerosol}$ for calculation of k_{het} via Eq. (3).

In addition to this continuous sequence, diagnostic tests were preformed once a day to directly determine the magnitude of k_{wall}, by injecting N_2O_5 to the top and then bottom of the flow reactor in the absence of particles. The sampling cycle described here was controlled autonomously by a custom LabView program.

Beyond the advantage of boosting S_a concentrations, laboratory experiments have the ability to control (or eliminate) secondary effects of temperature, RH, and trace gas biases, which is obviously not the case for field measurements. Measurements of $\gamma(N_2O_5)$ were most influenced by the rapid changes in temperature and RH that occurred in the early morning and late afternoons. As discussed previously, changes in RH on the time scale of the sampling cycle effect the retrieved $\gamma(N_2O_5)$ by altering the baseline k_{wall}. Changes in temperature effect the retrieved $\gamma(N_2O_5)$ by altering the N_2O_5-NO_3 ratio, and are most significant when ambient temperature fluctuates on the time scale of the observation above 25°C, due to the strong temperature dependence of the N_2O_5-NO_3 equilibrium. In addition, local sources of NO have the potential to upset the $\gamma(N_2O_5)$ measurement via titration of NO_3 as can be seen in Fig. 10, where a typical sampling cycle is disturbed by fresh NO emissions from an idling truck adjacent to the sampling tower. The coincident measurements of NO illustrate that the $\gamma(N_2O_5)$ measurement is well buffered at NO mixing ratios below 1 ppbv, but is significantly affected by elevated levels of NO (>1 ppbv). Cases where the $\gamma(N_2O_5)$ measurement was affected by extreme fluctuations in NO, temperature and RH, were diagnosed by both direct co-located observations of these quantities and deviations in the expected decay of N_2O_5 in the flow reactor, and these cases were subsequently removed from the analysis.

In summary, we made 205 measurements of $\gamma(N_2O_5)$ over the course of 18 days in Boulder, CO. Of which, 20% (43 observations) met the sampling criteria outlined in the previous section. The most accurate determinations of $\gamma(N_2O_5)$ were made at night when both temperature and RH were more constant and the influence of local NO emissions was muted due to minimal local traffic. The observed point-to-point variability, ±0.005, in $\gamma(N_2O_5)$ measured on particles of similar chemical composition at similar RH was consistent with the uncertainty described in Sect. 4. The ensemble mean $\gamma(N_2O_5)$ for the Boulder observations was 0.006±0.002, reflective of the low RH (30±15%) and high POM mass fraction (>0.6). These observations are discussed in detail in Bertram et al. (2009).

7 Conclusions and future directions

We report a new experimental approach for measuring the reactivity of trace gases with ambient aerosol particles. We describe the reactivity measurement with application towards N_2O_5 uptake and determine an upper limit to the single-point uncertainty in $\gamma(N_2O_5)$ of $\pm(1.3\times10^{-2}+0.2\times\gamma(N_2O_5))$ for S_a=100 μm^2 cm^{-3}, decreasing to $\pm(1.3\times10^{-3}+0.2\times\gamma(N_2O_5))$ for S_a=1000 μm^2 cm^{-3}. The experimental method for determining $\gamma(N_2O_5)$ was investigated in the laboratory on particles of known reactivity, at S_a concentrations representative of the troposphere. Measurements of $\gamma(N_2O_5)$ on MA particles determined in this study agree with previous laboratory observations over a range of RH and particle phase states to within ±20%. We discuss the uncertainty of the retrieved reaction probabilities in the context of fluctuations in ambient temperature, RH and trace gases, and comment on the ideal sampling conditions for measurement of $\gamma(N_2O_5)$.

Scientific results from two field deployments designed to determine the primary drivers for variability in $\gamma(N_2O_5)$ are discussed elsewhere. Future experiments using the entrained aerosol flow reactor can and will likely include: i) measurement of the gas-phase reactivity of NO_3 to fully investigate nocturnal nitrogen processing, ii) determination of the $ClNO_2$ yield following uptake of N_2O_5 on chloride containing particles (McNeill et al., 2006; Thornton and Abbatt, 2005b), and iii) investigation of the reactivity of other trace gases of tropospheric significance (e.g., HO_2, HNO_3, HOBr) on ambient particles (Thornton and Abbatt, 2005a).

Acknowledgements. This work was funded in large part by a grant from the Office of Earth Science (NIP/03-0000-0025) at the National Aeronautics and Space Administration. THB gratefully acknowledges the NOAA Climate and Global Change Fellowship Program for financial support. We thank Brian Lerner and Eric Williams (NOAA ESRL) for meteorological and NO data and Charles A. Brock (NOAA ESRL) for S_a data during the Boulder observations, and Timothy S. Bates and Patricia Quinn (NOAA PMEL) for S_a data during the Seattle observations.

References

Abbatt, J. P. D. and Waschewsky, G. C. G.: Heterogeneous interactions of HOBr, HNO_3, O_3, and NO_2 with deliquescent NaCl aerosols at room temperature, J. Phys. Chem. A, 102, 3719–3725, 1998.

Atkinson, R. and Arey, J.: Gas-phase tropospheric chemistry of biogenic volatile organic compounds: a review, Atmos. Environ., 37, S197–S219, 2003.

Badger, C. L., Griffiths, P. T., George, I., Abbatt, J. P. D., and Cox, R. A.: Reactive uptake of N_2O_5 by aerosol particles containing mixtures of humic acid and ammonium sulfate, J. Phys. Chem. A, 110, 6986–6994, 2006.

Behnke, W. and Zetzsch, C.: Heterogeneous formation of chlorine atoms from various aerosols in the presence of O_3 and HCl, J. Aerosol Sci., 20, 1167–1170, 1989.

Bertram, T. H., Thornton, J. A., Riedel, T., Middlebrook, A. M., Bahreini, R., Brock, C. A., Bates, T. S., Quinn, P. K., and Coffman, D.: A controlling role for particulate organic matter in regulating NO_x availability and tropospheric ozone production, Nature Geoscience, submitted, 2009.

Boulter, J. E., Cziczo, D. J., Middlebrook, A. M., Thomson, D. S., and Murphy, D. M.: Design and performance of a pumped counterflow virtual impactor, Aerosol Sci. Technol., 40, 969–976, 2006.

Braban, C. F. and Abbatt, J. P. D.: A study of the phase transition behavior of internally mixed ammonium sulfate - malonic acid aerosols, Atmos. Chem. Phys., 4, 1451–1459, 2004, http://www.atmos-chem-phys.net/4/1451/2004/.

Broekhuizen, K. E., Thornberry, T., Kumar, P. P., and Abbatt, J. P. D.: Formation of cloud condensation nuclei by oxidative processing: Unsaturated fatty acids, J. Geophys. Res., 109, D24206, doi:10.1029/2004JD005298, 2004.

Brown, R. L.: Tubular Flow Reactors with 1st-Order Kinetics, Journal of Research of the National Bureau of Standards, 83, 1–8, 1978.

Brown, S. S., Ryerson, T. B., Wollny, A. G., Brock, C. A., Peltier, R., Sullivan, A. P., Weber, R. J., Dube, W. P., Trainer, M., Meagher, J. F., Fehsenfeld, F. C., and Ravishankara, A. R.: Variability in nocturnal nitrogen oxide processing and its role in regional air quality, Science, 311, 67–70, 2006.

Calvert, J. G., Lazrus, A., Kok, G. L., Heikes, B. G., Walega, J. G., Lind, J., and Cantrell, C. A.: Chemical Mechanisms of Acid Generation in the Troposphere, Nature, 317, 27–35, 1985.

Cosman, L. M. and Bertram, A. K.: Reactive uptake of N_2O_5 on aqueous H_2SO_4 solutions coated with 1-component and 2-component monolayers, J. Phys. Chem. A, 112, 4625–4635, 2008.

Cosman, L. M., Knopf, D. A., and Bertram, A. K.: N_2O_5 reactive uptake on aqueous sulfuric acid solutions coated with branched and straight-chain insoluble organic surfactants, J. Phys.

Chem. A, 112, 2386–2396, 2008.

Dentener, F. J. and Crutzen, P. J.: Reaction of N_2O_5 on tropospheric aerosols - Impact on the global distributions of NO_x, O_3, and OH, J. Geophys. Res., 98, 7149–7163, 1993.

Evans, M. J. and Jacob, D. J.: Impact of new laboratory studies of N_2O_5 hydrolysis on global model budgets of tropospheric nitrogen oxides, ozone, and OH, Geophys. Res. Lett., 32, L09813, doi:10.1029/2005GL022469, 2005.

Finlayson-Pitts, B. J., Ezell, M. J., and Pitts, J. N.: Formation of chemically active chlorine compounds by reactions of atmospheric NaCl particles with gaseous N_2O_5 and $ClONO_2$, Nature, 337, 241–244, 1989.

Folkers, M., Mentel, T. F., and Wahner, A.: Influence of an organic coating on the reactivity of aqueous aerosols probed by the heterogeneous hydrolysis of N_2O_5, Geophys. Res. Lett., 30(12), p. 1644, doi:10.1029/2003GL017168, 2003.

Fried, A., Henry, B. E., Calvert, J. G., and Mozurkewich, M.: The reaction probability of N_2O_5 with sulfuric-acid aerosols at stratospheric temperatures and compositions, J. Geophys. Res., 99, 3517–3532, 1994.

George, I. J., Vlasenko, A., Slowik, J. G., Broekhuizen, K., and Abbatt, J. P. D.: Heterogeneous oxidation of saturated organic aerosols by hydroxyl radicals: uptake kinetics, condensed-phase products, and particle size change, Atmos. Chem. Phys., 7, 4187–4201, 2007, http://www.atmos-chem-phys.net/7/4187/2007/.

Gross, S. and Bertram, A. K.: Reactive uptake of NO_3, N_2O_5, NO_2, HNO_3, and O_3 on three types of polycyclic aromatic hydrocarbon surfaces, J. Phys. Chem. A, 112, 3104–3113, 2008.

Hanson, D. and Kosciuch, E.: The NH_3 mass accommodation coefficient for uptake onto sulfuric acid solutions, J. Phys. Chem. A, 107, 2199–2208, 2003.

Hu, J. H. and Abbatt, J. P. D.: Reaction probabilities for N_2O_5 hydrolysis on sulfuric acid and ammonium sulfate aerosols at room temperature, J. Phys. Chem. A, 101, 871–878, 1997.

Jang, M. S., Czoschke, N. M., Lee, S., and Kamens, R. M.: Heterogeneous atmospheric aerosol production by acid-catalyzed particle-phase reactions, Science, 298, 814–817, 2002.

Jayne, J. T., Leard, D. C., Zhang, X. F., Davidovits, P., Smith, K. A., Kolb, C. E., and Worsnop, D. R.: Development of an aerosol mass spectrometer for size and composition analysis of submicron particles, Aerosol Sci. Technol., 33, 49–70, 2000.

Kercher, J. P., Riedel, T. P., and Thornton, J. A.: Chlorine activation by N_2O_5: simultaneous, in situ detection of $ClNO_2$ and N_2O_5 by chemical ionization mass spectrometry, Atmos. Meas. Tech. Discuss., 2, 119–151, 2009, http://www.atmos-meas-tech-discuss.net/2/119/2009/.

Kroll, J. H. and Seinfeld, J. H.: Representation of secondary organic aerosol laboratory chamber data for the interpretation of mechanisms of particle growth, Environ. Sci. Technol., 39, 4159–4165, 2005.

Laskin, A., Wang, H., Robertson, W. H., Cowin, J. P., Ezell, M. J., and Finlayson-Pitts, B. J.: A new approach to determining gas-particle reaction probabilities and application to the heterogeneous reaction of deliquesced sodium chloride particles with gas-phase hydroxyl radicals, J. Phys. Chem. A, 110, 10619–10627, 2006.

Mak, J., Gross, S., and Bertram, A. K.: Uptake of NO_3 on soot and pyrene surfaces, Geophys. Res. Lett., 34, L10804, doi:10.1029/2007GL029756, 2007.

Martin, S. T., Rosenoern, T., Chen, Q., and Collins, D. R.: Phase Changes of Ambient Particles in the Southern Great Plains of Oklahoma, USA, Geophys. Res. Lett., 35, L22801, doi:10.1029/2008GL035650, 2008.

McNeill, V. F., Patterson, J., Wolfe, G. M., and Thornton, J. A.: The effect of varying levels of surfactant on the reactive uptake of N_2O_5 to aqueous aerosol, Atmos. Chem. Phys., 6, 1635–1644, 2006, http://www.atmos-chem-phys.net/6/1635/2006/.

McNeill, V. F., Yatavelli, R. L. N., Stipe, C. B., and Landgrebe, O.: Heterogeneous OH oxidation of palmitic acid in single component and internally mixed aerosol particles: vaporization and the role of particle phase, Atmos. Chem. Phys., 8, 5465–5476, 2008, http://www.atmos-chem-phys.net/8/5465/2008/.

Mentel, T. F., Sohn, M., and Wahner, A.: Nitrate effect in the heterogeneous hydrolysis of dinitrogen pentoxide on aqueous aerosols, PCCP, 1, 5451–5457, 1999.

Molina, M. J., Ivanov, A. V., Trakhtenberg, S., and Molina, L. T.: Atmospheric evolution of organic aerosol, Geophys. Res. Lett., 31, L22104, doi:10.1029/2004GL020910, 2004.

Mozurkewich, M. and Calvert, J. G.: Reaction probability of N_2O_5 on aqueous aerosols, J. Geophys. Res., 93, 15889–15896, 1988.

Murphy, D. M. and Thomson, D. S.: Laser Ionization Mass-Spectroscopy of Single Aerosol-Particles, Aerosol Sci. Technol., 22, 237–249, 1995.

Osthoff, H. D., Roberts, J. M., Ravishankara, A. R., Williams, E. J., Lerner, B. M., Sommariva, R., Bates, T. S., Coffman, D., Quinn, P. K., Dibb, J. E., Stark, H., Burkholder, J. B., Talukdar,

R. K., Meagher, J., Fehsenfeld, F. C., and Brown, S. S.: High levels of nitryl chloride in the polluted subtropical marine boundary layer, Nature Geoscience, 1, 324–328, 2008.

Park, S. C., Burden, D. K., and Nathanson, G. M.: The inhibition of N_2O_5 hydrolysis in sulfuric acid by 1-butanol and 1-hexanol surfactant coatings, J. Phys. Chem. A, 111, 2921–2929, 2007.

Ravishankara, A. R.: Heterogeneous and multiphase chemistry in the troposphere, Science, 276, 1058–1065, 1997.

Robinson, G. N., Worsnop, D. R., Jayne, J. T., Kolb, C. E., and Davidovits, P.: Heterogeneous uptake of $ClONO_2$ and N_2O_5 by sulfuric acid solutions, J. Geophys. Res., 102, 3583–3601, 1997.

Sioutas, C., Koutrakis, P., Ferguson, S. T., and Burton, R. M.: Development and Evaluation of a Prototype Ambient Particle Concentrator for Inhalation Exposure Studies, Inhalation Toxicology, 7, 633–644, 1995.

Thornton, J. and Abbatt, J. P. D.: Measurements of HO_2 uptake to aqueous aerosol: Mass accommodation coefficients and net reactive loss, J. Geophys. Res., 110, D08309, doi:10.1029/2004JD005402, 2005a.

Thornton, J. A. and Abbatt, J. P. D.: N_2O_5 reaction on submicron sea salt aerosol: Kinetics, products, and the effect of surface active organics, J. Phys. Chem. A, 109, 10004–10012, 2005b.

Thornton, J. A., Braban, C. F., and Abbatt, J. P. D.: N_2O_5 hydrolysis on sub-micron organic aerosols: the effect of relative humidity, particle phase, and particle size, PCCP, 5, 4593–4603, 2003.

Vlasenko, A., George, I. J., and Abbatt, J. P. D.: Formation of volatile organic compounds in the heterogeneous oxidation of condensed-phase organic films by gas-phase OH, J. Phys. Chem. A, 112, 1552–1560, 2008.

Vogt, R. and Finlayson-Pitts, B. J.: A Diffuse-Reflectance Infrared Fourier-Transform Spectroscopic (Drifts) Study of the Surface-Reaction of NaCl with Gaseous NO_2 and HNO_3, J. Phys. Chem., 98, 3747–3755, 1994.

Wahner, A., Mentel, T. F., Sohn, M., and Stier, J.: Heterogeneous reaction of N_2O_5 on sodium nitrate aerosol, J. Geophys. Res., 103, 31103–31112, 1998.

Wang, J., Hoffmann, A. A., Park, R. J., Jacob, D. J., and Martin, S. T.: Global distribution of solid and aqueous sulfate aerosols: Effect of the hysteresis of particle phase transitions, J. Geophys. Res., 113, D11206, doi:10.1029/2007JD009367, 2008.

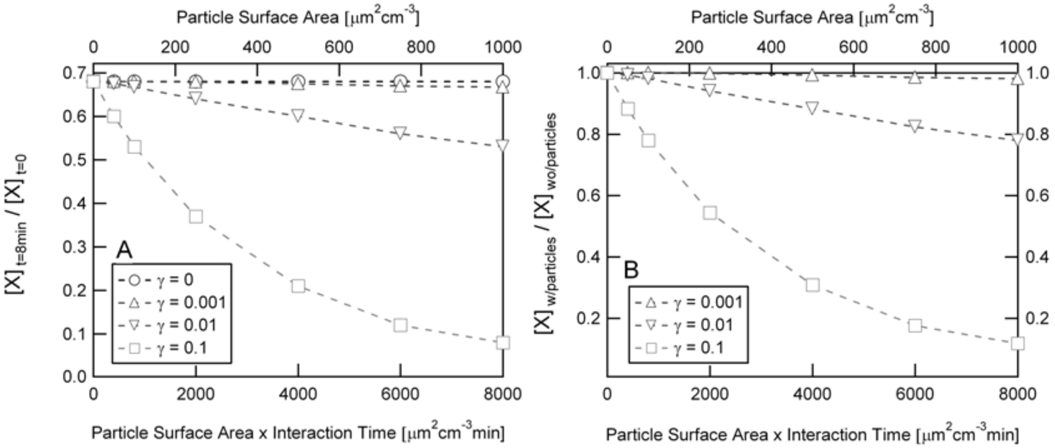

Fig. 1. Time-dependent box model simulations of the flow reactor chemistry, assuming k_{wall}=2.5×10^{-3} s^{-1} and Δt=8 min for three representative reaction probabilities (γ=0.001, 0.01, and 0.1). The concentration at the base of the reactor, $[X]_{t=8\,\mathrm{min}}$, is shown in panel **(A)** relative to the initial concentration at the top of the flow reactor, $[X]_{t=0\,\mathrm{min}}$. The ratio of $[X]$ measured in the presence of particles to that in the absence of particles, as a function of γ, is shown in panel **(B)**. The solid line in panel (B) corresponds to γ=0.

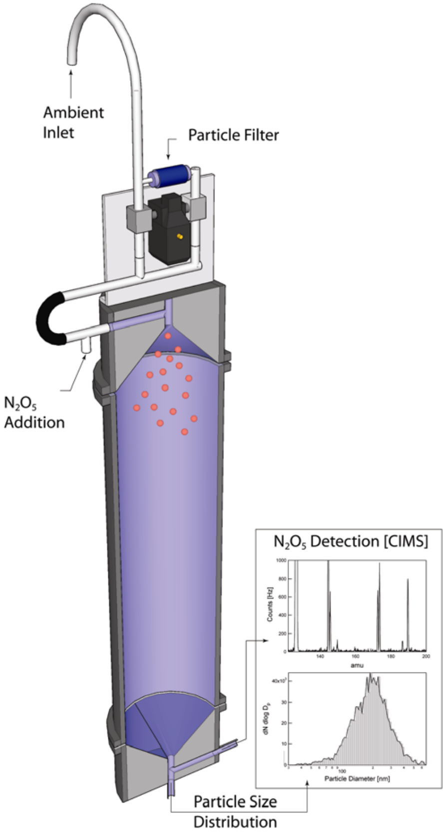

Fig. 2. Schematic of the entrained aerosol flow reactor.

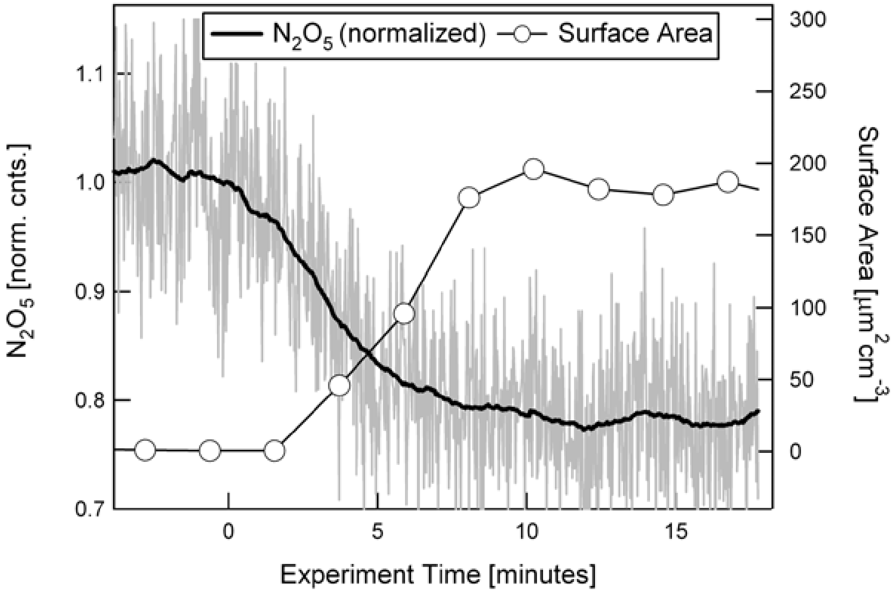

Fig. 3. Observed decay in N_2O_5 (gray) and rise in particle surface area concentration (open circles) detected at the base of the flow reactor following the removal of the inlet filter (at time=0). The covariance between N_2O_5 and SA concentration is indicative of N_2O_5 uptake on the injected particles (aqueous malonic acid). The transit time of the particle-laden air confirms an average reaction time of eight minutes predicted by the flow conditions and chamber dimensions.

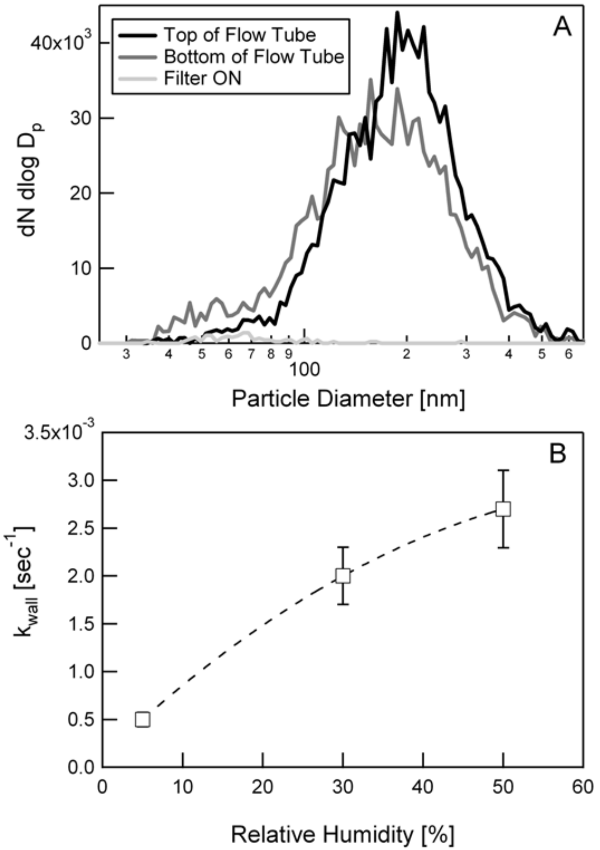

Fig. 4. Particle and N_2O_5 transmission. **(A)** Particle size distributions of laboratory generated particles measured at the top (black) and base (dark gray) of the flow reactor with the inlet filter bypassed and with the inlet filter inline (light gray). **(B)** Relative humidity dependence in the measured pseudo-first-order wall loss rate coefficient (k_{wall}) of N_2O_5 in the halocarbon coated flow reactor.

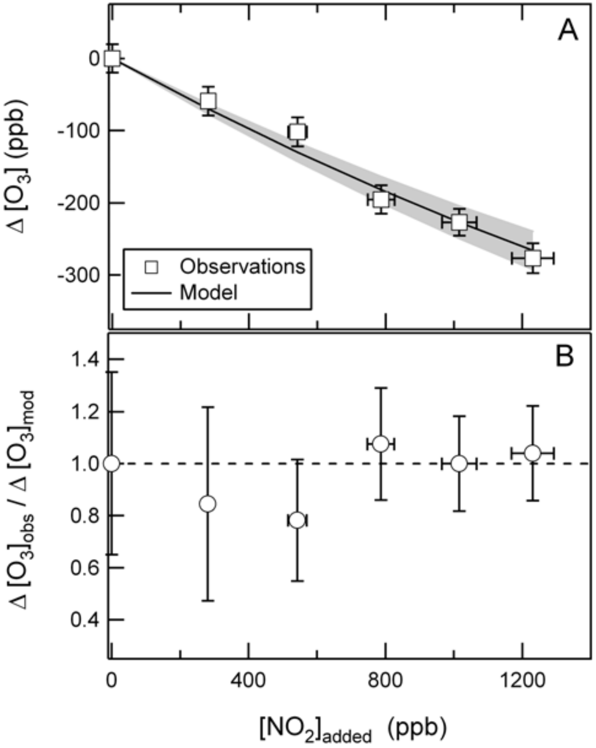

Fig. 5. Characterization of the N_2O_5 source. **(A)** Observed (squares) and predicted (line) changes in O_3 following addition of NO_2 to the source flow tube. The shaded region represents the combined uncertainty in the model, stemming from uncertainty in the reaction time and NO_2cylinder concentration. The change in O_3 is equal to the production of N_2O_5 (R1–R2). Observations and model analysis are for the undiluted source. **(B)** Ratio of the observed to modeled change in O_3 as a function of NO_2. The results confirm that we can predict the concentration of N_2O_5 produced in the generation source to within ±20%.

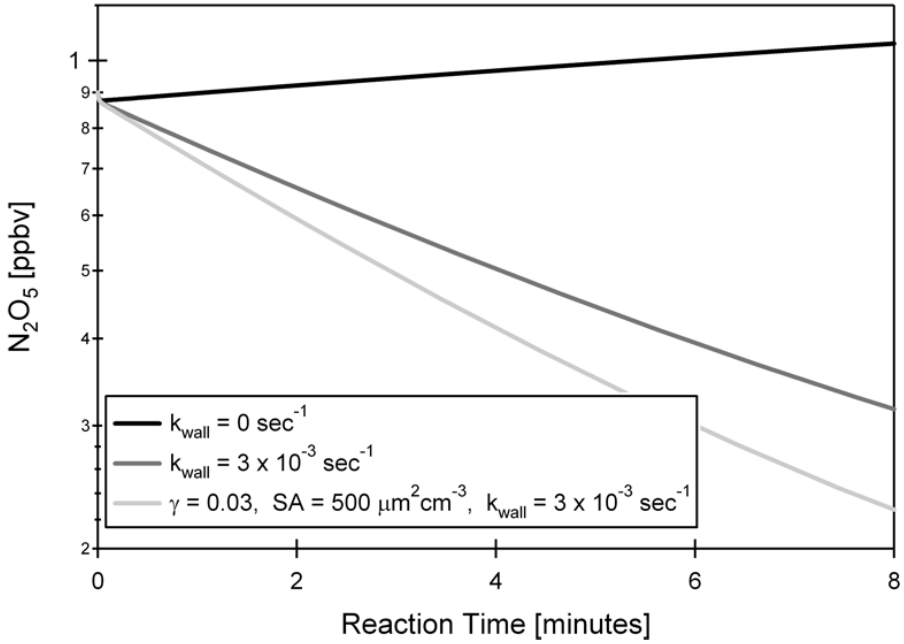

Fig. 6. Modeled decay in N_2O_5, calculated using a time-dependent box model, assuming initial concentrations of NO_2, O_3 and N_2O_5 of 50, 10, and 1 ppbv, respectively. Net production of N_2O_5 is observed when $k_{\text{wall}}=0\,s^{-1}$ (black line). The ratio between the decay observed in the presence (light gray line) and absence (dark gray line) of particles, measured at $\Delta t=8$ min is directly related to k_{het} via Eq. (3).

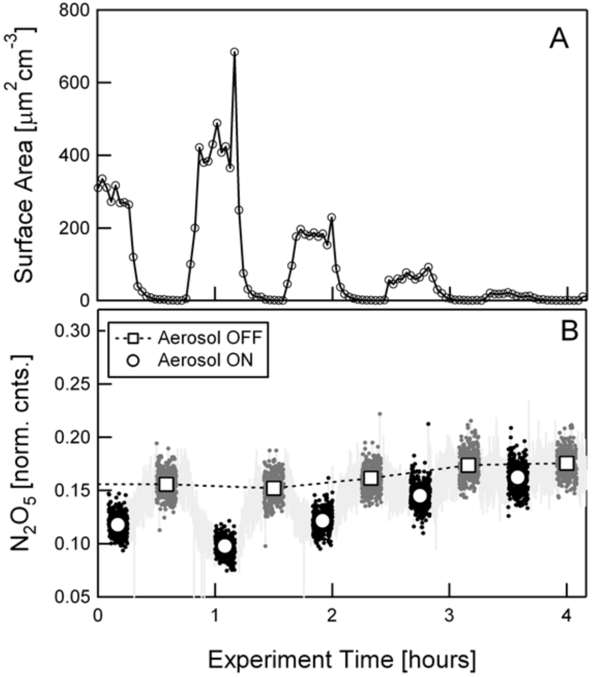

Fig. 7. Time series in particle surface area concentration **(A)** and N_2O_5 **(B)** measured at the base of the flow reactor during a typical sampling sequence where particles are modulated on and off using an inlet filter. Ten minute binned means for N_2O_5 are shown for the filter inline (gray squares) and filter bypassed (black circles) in panel (B).

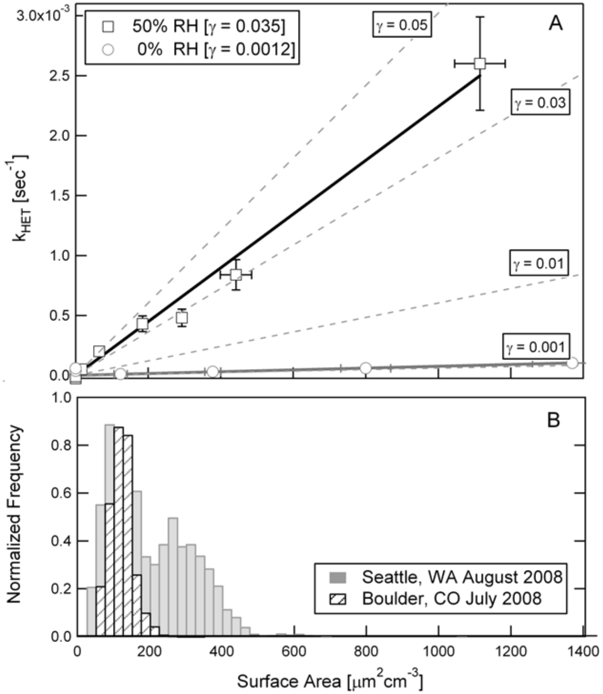

Fig. 8. (A) Measured first-order rate coefficients (k_{het}) for the decay of N_2O_5 in the presence of aqueous (black squares) and crystalline (gray circles) malonic acid particles as a function of particle surface area concentration. The solid lines represent least squares fits of the observed data points. Dashed lines show representative slopes for various values of $\gamma(N_2O_5)$. **(B)** Normalized frequency distribution for ambient measurements of particle surface area concentration made in Boulder, CO (black dashed boxes) and Seattle, WA (solid gray boxes).

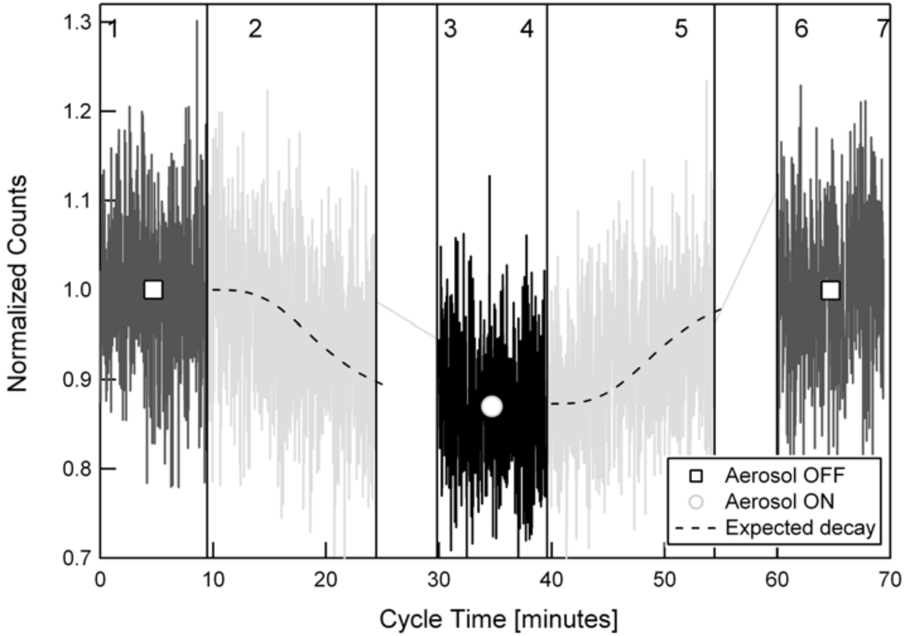

Fig. 9. Typical sampling cycle for the reactivity measurement as conducted under ambient conditions in Boulder, CO. Detailed discussion of each step can be found in Sect. 6. Note: The reaction time employed in Boulder, CO was slightly longer than the typical 8 min interaction time described in the text.

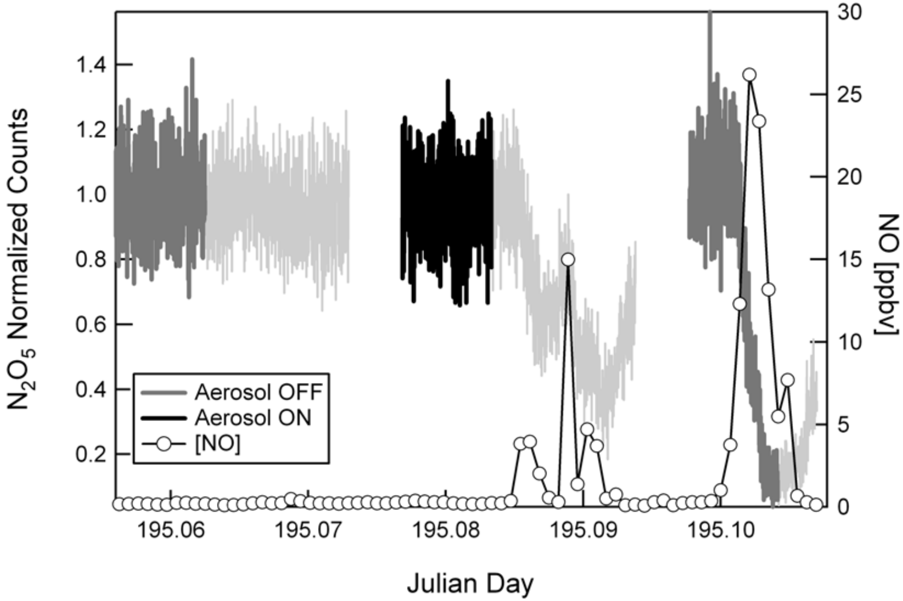

Fig. 10. Example of an ambient reactivity measurement severely influenced by local NO emissions.